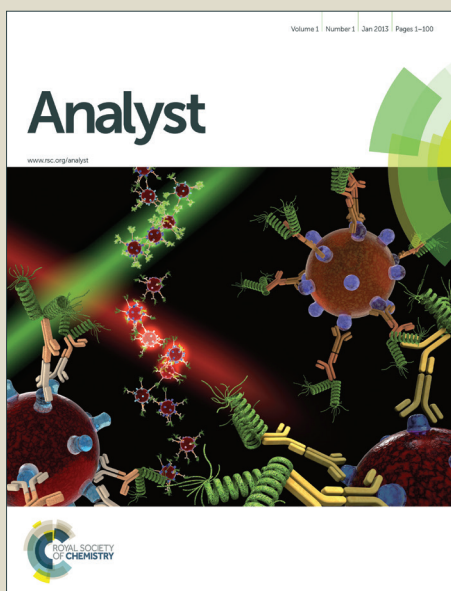


Analyst

Accepted Manuscript



This is an *Accepted Manuscript*, which has been through the Royal Society of Chemistry peer review process and has been accepted for publication.

Accepted Manuscripts are published online shortly after acceptance, before technical editing, formatting and proof reading. Using this free service, authors can make their results available to the community, in citable form, before we publish the edited article. We will replace this *Accepted Manuscript* with the edited and formatted *Advance Article* as soon as it is available.

You can find more information about *Accepted Manuscripts* in the [Information for Authors](#).

Please note that technical editing may introduce minor changes to the text and/or graphics, which may alter content. The journal's standard [Terms & Conditions](#) and the [Ethical guidelines](#) still apply. In no event shall the Royal Society of Chemistry be held responsible for any errors or omissions in this *Accepted Manuscript* or any consequences arising from the use of any information it contains.

Ion-Transfer Voltammetric Determination of Folic Acid at the Meso-Liquid/Liquid Interface Arrays

Xuheng Jiang, Kui Gao, Daopan Hu, Huanhuan Wang, Shujuan Bian, Yong Chen*

*School of Chemical and Environmental Engineering, Shanghai Institute of Technology,
Shanghai 201418, China*

Abstract

Voltammetric studies on the simple ion transfer (IT) behaviors of an important water-soluble B-vitamin, folic acid (FA), at the liquid/liquid (L/L) interface were firstly performed and applied as a novel detection method for FA under physiological conditions. Meso-water/1,6-dichlorohexane (W/DCH) and meso-water/organogel interface arrays were built by using a hybrid mesoporous silica membrane (HMSM) with unique structure of pores-in-pores and employed as the new platforms for the IT voltammetric study. In view of the unique structure of such a HMSM, the impact of ionic surfactant cetyltrimethylammonium bromide (CTAB) self-assembled within the silica nanochannels of HMSM on the IT voltammetric behavior and detection of FA at the meso-L/L interface arrays was systematically examined by cyclic voltammetry (CV), differential pulse voltammetry (DPV) and differential pulse stripping voltammetry (DPSV). It is found that all the voltammetric responses of CV, DPV, and DPSV and the corresponding detection limit of FA at such meso-L/L interface arrays are closely related to the CTAB in HMSM. Significantly, the calculated detection limit of FA could be improved to 80 nM after the combination of DPSV technique with the additional preconcentration of FA in the silica-CTAB nanochannels through an anion-exchange process between FA⁻ and the bromide of CTAB in HMSM, which provides a new and attractive strategy for the detection of those biological anions.

* Corresponding Author. Tel: +81-21-6087-3563; fax: +81-21-6087-3563
E-mail address: yongchen@sit.edu.cn

1
2
3
4
5
6
7
8
9
10
11
12
13
14
15
16
17
18
19
20
21
22
23
24
25
26
27
28
29
30
31
32
33
34
35
36
37
38
39
40
41
42
43
44
45
46
47
48
49
50
51
52
53
54
55
56
57
58
59
60

Keywords: Folic Acid, Determination, Mesoporous membrane, Liquid/liquid interface, Ion transfer, Voltammetry

Introduction

Folic acid (FA) is an important water-soluble B-vitamin, in general recognized as one of the most important vitamin for normal metabolic function in human beings, which participates in numerous reactions occurring in the body.¹ Especially, it is involved in the development of the tissues and brain of a fetus and growth of a baby, but its mean intake was found to be lower than recommended in many countries.^{1,2} Therefore, there has always been the tremendous interest focused on the development of simple, sensitive and accurate methods for the determinations of FA in pharmaceutical, clinical and food samples.³⁻¹⁴ During the past decade, numerous analytical methods have been developed for the determination of FA, including enzyme-linked immunosorbent assays (ELISAs),⁴ high-performance liquid chromatography (HPLC),⁵ HPLC-MS,⁶ capillary electrophoresis (CE)⁷ and spectrophotometry methods.⁸ Although those methods offer high sensitivity (S) and low limit of detection (LOD), most of them suffer from disadvantages such as expensive instruments and time-consuming procedure. Thus, electrochemical detection of FA has recently become progressively attractive and it is attaining significant attention because the electroanalysis procedures are relatively simple and electrochemical devices are uncomplicated and inexpensive, which is apt to be miniaturized for the portable electrochemical sensors.^{3,9,10} Till date, all electroanalytical studies on FA have only focused on the redox or adsorption/desorption reactions of FA occurring at mercury^{11,12} or other solid electrodes.^{3,13,14} Nevertheless, some of the electrodes, such as mercury and lead electrode,^{3,11} are harmful for the environment and the health of the human beings. Therefore, it is significant to further explore other detection methods for FA.

Over the last three decades, ion transfer (IT) voltammetry relying on the IT across a polarized liquid/liquid (L/L) interface (the interface between two immiscible electrolyte solutions (ITIES) or the oil/water interface (O/W)) has been extensively

1
2
3 used to investigate the IT reactions of various inorganic and organic ions for their
4 quantitative determinations.¹⁵⁻¹⁷ Notably, the electroanalytical performances can be
5 significantly improved by miniaturizing the electrified interface for the
6 highly-sensitive detection of many ions¹⁸⁻³⁵ because miniaturization of L/L interface
7 can effectively eliminate some severe problems often found at the conventionally
8 large L/L interface (mm-size), such as too large iR -drop and charging current.¹⁸
9 Among the development of micro-L/L interface electrochemistry, electrochemical
10 studies of IT behaviors at the arrays of micro-L/L interface (μ -L/L arrays) supported
11 by versatile porous membranes, such as zeolite,^{28,29} porous anodic alumina,^{30,31}
12 track-etched polymer membranes^{32,33} and silicon chips³⁴⁻³⁶ have recently attracted
13 significant attention for the detections of some biological ions, for example,
14 lysozyme,³⁷ dopamine,³⁸ noradrenaline,³⁹ and ionic drugs⁴⁰ at the arrays of
15 micro-oil/water interface, as well as oligopeptides⁴¹, β -blocker propranolol,⁴²
16 hen-egg-white-lysozyme,³⁴ rat amylin⁴³ and insulin⁴⁴ etc, at the arrays of
17 μ -water/organogel interface after gelation of organic electrolyte phase. According to
18 the literatures, the IT voltammetric behaviors and the corresponding detection
19 performances at μ -L/L arrays are closely related to the structure of employed porous
20 membrane^{28-36,45} and the different sensitivity of various voltammetric techniques.⁴¹⁻⁴⁴
21 Since that, it is necessary to exploit more porous membranes with different structure
22 and properties as the supporters to build μ -L/L arrays for the highly-sensitive
23 detection of biological ions using versatile voltammetric techniques. Recently, a novel
24 polyethylene terephthalate (PET)-templated hybrid mesoporous silica membrane
25 (HMSM) with unique structure of pores-in-pores and meso-sized selectivity has been
26 successfully synthesized and applied to support the meso-water/1,2-dichloroethane
27 (W/DCE) interface arrays for the size-selective ion transfer or extraction in our
28 group.⁴⁶ Moreover, such a PET-templated HMSM can be further applied to
29 electrochemically fabricate a membrane electric-device based on the electrochemistry
30 at the membrane-supported L/L interface by Huang et al.⁴⁷
31
32
33
34
35
36
37
38
39
40
41
42
43
44
45
46
47
48
49
50
51
52
53
54
55

56 The above mentioned results inspired us to further apply such a HMSM in the
57
58
59
60

1
2
3
4
5
6
7
8
9
10
11
12
13
14
15
16
17
18
19
20
21
22
23
24
25
26
27
28
29
30
31
32
33
34
35
36
37
38
39
40
41
42
43
44
45
46
47
48
49
50
51
52
53
54
55
56
57
58
59
60

ion-transfer voltammetric studies for the determination of biological substrates, such as FA. Herein, the voltammetric studies on the simple IT behaviors of FA were firstly performed for the quantitative determinations of FA at two types of meso-L/L interface arrays, namely meso-water/1,6-dichlorohexane (W/DCH) and meso-water/organogel interface arrays supported by using the PET-templated HMSM.⁴⁶ The main objective of this study was to systematically investigate the IT processes of FA at the meso-L/L interface arrays by employing different voltammetric techniques and then to explore a novel detection method for FA relying on its IT reaction at the L/L interface.

Experimental section

Reagents and Membrane Materials. Folic acid (A.R), chemically known as [N-(4-{[2-amino-1,4-dihydro-4-oxo-6-pteridiny]methyl}amino)benzoyl]-L-glutamic acid], which is represented in scheme 1, was purchased from Sinopharm, China and was used without any further purification. The organic electrolyte salt used in this study was the bis(triphenylphosphoranylidene) ammonium tetrakis(4-chlorophenyl)borate (BTTPATPBCl), which was prepared using bis(triphenylphosphoranylidene) ammonium chloride (BTTPACl, 97%, Sigma-Aldrich, USA) and potassium tetrakis(4-chlorophenyl)-borate (KTPBCl, 98%, Acros, USA). Tetramethylammonium chloride ($\geq 99.0\%$) was purchased from Sinopharm, China. The organic phase solution 1,6-dichlorohexane (1,6-DCH, 98%) was purchased from Aldrich and was purified according to the published procedure.⁴⁸ The organogel phase was prepared using purified 1,6-DCH and low-molecular weight polyvinylchloride (PVC) as described in the literature.⁴¹ Other chemicals used for the preparation of supporting electrolytes were sodium chloride (NaCl, Sinopharm, China), potassium phosphate monobasic (KH₂PO₄, Sinopharm, China) and sodium hydroxide (NaOH, Sinopharm, China). The chemicals used in the interference investigation were ascorbic acid (99%, Aldrich), NaClO₄ (Sinopharm, China), NaAc (Sinopharm, China), KSCN (Sinopharm, China), and Na₂SO₄ (Sinopharm, China). Aqueous solution were prepared in purified water, with a

1
2
3 resistivity of 18 MΩ cm. Aqueous supporting electrolytes solution in the studies was 0.1
4 M KH₂PO₄ and 0.1 M NaOH buffer (for pH 7.2).
5
6

7
8 Porous PET membranes with pore diameter of 1 μm, thickness of 5 μm and
9 porosity of ~1% were obtained from Haoxia Nuclepore membrane Ltd, China.
10 According to our previous report,⁴⁶ the CTAB-containing HMSM and the HMSM
11 without CTAB were prepared by the aspiration-induced infiltration method with or
12 without solvent-extraction and abbreviated herein as HMSM-CTAB and HMSM,
13 respectively. The SEM image of as-synthesized HMSM revealed the formation of
14 numerous rod-like materials inside the channel of PET membrane (Fig. 1), which was
15 similar to the phenomena as reported previously.⁴⁶
16
17

18
19 Preparation of Standard and Sample solutions of FA. All the standard and sample
20 solutions of FA were prepared daily using phosphate buffer solution and stored in the
21 dark until used because FA undergoes photodegradation by ultraviolet radiation in
22 aqueous solution.⁴⁹ The pharmaceutical preparations analyzed were Folovit tablets
23 produced by Beijing Scrianen Pharmaceutical Co., Ltd., containing 0.4 mg of FA in
24 each tablet. One tablet was pulverized thoroughly in a mortar. Subsequently, the powder
25 was transferred into a dry volumetric flask and ultrasonically dissolved in water to
26 obtain aqueous solution. The contents were centrifuged for 10 minutes and the
27 supernatant was transferred into a 100 mL volumetric flask and the volume was made
28 up with the phosphate buffer solution to 100 mL. 10 mL of this solution was diluted by
29 phosphate buffer solution to 50 mL for the final sample solution of FA.
30
31
32
33
34
35
36
37
38
39
40
41
42
43
44

45 Voltammetry Experiments. All the voltammetric experiments at the meso-L/L
46 interface arrays were performed by a potentiostat (CHI660D, CHI, USA) and the
47 homemade four-electrode electrochemical cell was constructed according to the
48 methods described in literature^{41,46} (Supporting Information, SI, Fig. S1), where a pair
49 of Ag/AgCl electrodes (one in each phase) worked as reference electrodes controlling
50 the potential and a pair of Pt-wire electrodes (one in each phase) acted as counter
51 electrodes measuring the current. The Cell 1 and Cell 2 respectively used to study the
52 transfer of FA under physiological condition across the meso-W/DCH interface arrays
53
54
55
56
57
58
59
60

1
2
3 or the meso-water/organogel interface arrays are shown in Scheme 2. Voltammetric
4 behavior and detection of FA were examined by employing CV, DPV, and DPSV. DPV
5 and DPSV were used for analytical and detective studies with the following parameters
6 respectively at the meso-W/DCH interface arrays (DPV): pulse amplitude = 50 mV and
7 pulse width = 0.04 s, as well as at the water/organogel interface arrays (DPSV): the
8 amplitude of the pulse = 50 mV, sampling width = 0.03 s.
9
10
11
12
13

14
15 As for voltammetric detection of FA by employing DPSV, a preconditioning step
16 for the gel was implemented prior to each DPSV experiment. This involved the
17 application of a more positive potential compared to the transfer potential of the anions
18 being investigated for a period of time. The preconditioning potential of 0.8 V at an
19 applied preconditioning time of 90 s was selected as the optimized parameter.
20 Unextracted FA from previous run still present in the organogel was back-extracted into
21 the aqueous phase by this precondition step for cleaning the gel. In order to minimize
22 the contribution of background noise to the analytical signal, all the electrochemical
23 experiments were performed in a Faraday cage.
24
25
26
27
28
29
30
31
32
33
34

35 Results and discussion

36
37 Firstly, the IT behaviors of a reference ion, tetramethylammonium (TMA^+), at
38 the W/DCH interface supported by HMSM or HMSM-CTAB were studied prior to the
39 investigation of the IT reactions of FA at the same interface. As shown as Fig. 2A and
40 Fig. 2B, different CV responses are observed at the W/DCH interface supported by
41 different hybrid membranes. A typically asymmetric CV curve (Fig. 2A) is obtained at
42 the HMSM-supported W/DCH interface, namely, the CV response for the ion transfer
43 of TMA^+ from W to DCH is peak-shaped, while the CV response for its back transfer
44 from DCH to W is steady-stated. However, symmetrically peak-shaped CV curve (Fig.
45 2B) is obtained at the HMSM-CTAB-supported W/DCH interface, that is both of CV
46 responses for the IT of TMA^+ from W to DCH and its back transfer from DCH to W
47 are peak-shaped. Depending on the pH of aqueous solutions, FA exists in different ionic
48 states changing from the bi-cationic (FA^{2+}) form into cationic (FA^+), neutral (FA) and
49
50
51
52
53
54
55
56
57
58
59
60

1
2
3 anionic (FA^-) forms due to the different pK values of amino groups and carboxyl
4 groups of FA.⁵⁰ Under physiological conditions (pH~7.0), FA mainly existed in anionic
5 (FA^-) form.^{50,51} The typical examples for voltammetric behaviors of simple IT of FA^-
6
7 under physiological condition across both of the HMSM-supported and
8 HMSM-CTAB-supported meso-W/DCH interface arrays are shown as the CVs
9 displayed in Fig. 3. In the absence of the FA^- , only the capacitive current was observed
10 in the background CVs within the potential range of 0.1-0.8 V (the dashed lines in Fig.
11 3A and B). Fig. 3A and Fig. 3B exhibit the Faradic currents corresponding to the IT of
12 FA^- across both meso-W/DCH interface arrays in the presence of FA^- . However,
13 asymmetrical (Fig. 3A) and symmetric (Fig. 3B) CV curves are also respectively
14 obtained at the HMSM-supported and HMSM-CTAB-supported W/DCH interfaces. All
15 above different CV responses corresponding to the ITs of TMA^+ and FA^- at the W/DCE
16 interfaces supported by different HMSMs indicate that CTAB in HMSM can affect on
17 the voltammetric behaviors of IT of FA^- across such meso-W/DCH interface arrays, as
18 discussed in the followed part.
19
20
21
22
23
24
25
26
27
28
29
30
31

32 The investigation of pH of aqueous solution on the IT behaviors of FA was not
33 extensively investigated because of the poor solubility of FA in acidic solution (pH \leq
34 6.0) at room temperature.⁵² The results of DPV experiments conducted under neutral
35 and basic aqueous solution (SI Fig. S2) clearly demonstrate that the well-defined wave
36 corresponding to the IT behaviors of FA^- from W to DCH can be obtained at the pH
37 value ranging from 7.0 to 10.0, but the characteristic transfer wave of FA^- disappeared
38 when the pH value is around 11.0. This could be attributed to the poor-resistance of
39 silica to the basic solution,⁵³ leading to the possible destruction of meso-W/DCH
40 interface arrays. Comparing the SEM images of HMSM after the experiment conducted
41 under the condition of pH~11.0 (SI Fig. S3) to the image observed before DPV
42 experiment (Fig. 1B), it is found that silica rods in HMSM seems to be shrunken from
43 the membrane surface. Therefore, it is reasonable that the silica rods in HMSM were
44 partially dissolved in the relatively strong basic solution, leading to that
45 HMSM-supported W/DCH interface was partially blocked by the dissolved products.
46
47
48
49
50
51
52
53
54
55
56
57
58
59
60

1
2
3
4
5
6
7
8
9
10
11
12
13
14
15
16
17
18
19
20
21
22
23
24
25
26
27
28
29
30
31
32
33
34
35
36
37
38
39
40
41
42
43
44
45
46
47
48
49
50
51
52
53
54
55
56
57
58
59
60

Considering the main anionic state and the good uptake condition of FA in human body under physiological condition (pH~7.0),⁵⁴ the following voltammetric studies and detection of FA were only conducted at the physiological pH (~7.0), which should also be helpful to understand the transmembrane process of FA across biomembrane because L/L interface is considered as a simple model to mimic semi-biomembrane.¹⁵⁻¹⁸

Influence of CTAB in HMSM on IT Behaviors of FA⁻ across the Meso-W/DCH Interface Arrays. Fig. 3A and Fig. S4A display asymmetric CV curves corresponding to the IT of FA⁻ at the HMSM-supported W/DCH interface, which are distinct from the as-obtained symmetrically peak-shaped CV curves at the HMSM-CTAB-supported W/DCH interfaces (Fig. 3B and Fig. S4B). Based on our previous work on the IT across HMSM-supported W/DCE interface,⁴⁶ it is easy to understand the asymmetric CV curves for the ITs of TMA⁺ (Fig. 2A) or FA⁻ at the HMSM-supported W/DCH interface. Due to the hydrophilicity of silica nanochannels in HMSM after the removal of CTAB from HMSM,⁴⁶ the W/DCH interface supported by HMSM should form at the membrane surface and present asymmetric diffusion field, where the egress transfers of TMA⁺ or FA⁻ out of HMSM dominated by linear diffusion produces a peak-shaped CV response because of the confinement of silica nanochannels in HMSM, while the ingress transfers of TMA⁺ or FA⁻ into HMSM controlled by radial diffusion leads to a steady wave. Moreover, as found in our previous work on the simple ion transfer and the facilitated ion transfer across the HMSM-supported W/DCE interface, the effect of overlap of diffusion field on the voltammetric response often found in the membrane-supported-liquid/liquid interface electrochemistry can be ignored for such HMSM-supported liquid/liquid interface, because the normalized geometric parameter⁵⁵ ($K\lambda^{1/2}$) of HMSM-supported liquid/liquid interface was calculated herein about 2.33, which is less than 10. If the value of $K\lambda^{1/2}$ is larger than 10, the CV curves for the IT of TMA⁺ or FA⁻ at the HMSM-supported W/DCH interface should change from asymmetric shape to symmetrically peaked shape due to the transition from radial diffusion to linear diffusion field caused by the overlap of diffusion layers.⁵⁵

As for the HMSM-CTAB-supported W/DCH interface, as shown in Scheme 3A,

1
2
3 the W/DCH interface should form inside the hybrid membrane owing to the relatively
4 hydrophobic inner environment of silica-CTAB nanochannels caused by the alkyl chain
5 (cetyltrimethyl group) of CTAB.⁵⁶ Therefore, as shown as Fig. 3B and Fig. S4B, the
6 transfer of FA^- from W to DCH and its transfer back to the aqueous phase dominated by
7 linear diffusion produce the peak-shaped CV responses because of the confinement of
8 silica-CTAB nanochannels in HMSM. Also, the symmetrically peak-shaped CV
9 responses corresponding to the IT of TMA^+ at the HMSM-CTAB-supported W/DCH
10 interface (Fig. 2B) infers that the W/DCH interface should form inside the
11 HMSM-CTAB membrane. Although CTAB can be dissolved in some organic solvents,
12 the amount of dissolved CTAB from as-synthesized HMSM in the DCH phase of
13 HMSM-CTAB-supported W/DCH interface could be neglected because CTAB are
14 closely attached on the inner surface of silica-nanochannels as pointed out by the
15 previous reports^{56,57} on the CTAB-templated HMSM, which does not have obvious
16 impact on the IT experiments. Indeed, some results of electrochemical experiments
17 can support this viewpoint. On the one hand, if there are lots of dissolved cationic
18 surfactants, CTAB, at the HMSM-CTAB-supported W/DCH interface, it should be
19 possible to observe the instable electrochemical windows or the polarization curves
20 caused by the free cationic surfactants.^{58,59} However, it is obvious that no faradaic
21 current response appears and no electrochemical instability happens within the
22 background window (the dash lines in Fig. 2B and Fig. 3B). On the other hand, the
23 peak currents of continuous CVs corresponding to the IT of FA^- at the
24 HMSM-CTAB-supported W/DCH interface almost keep the constant with the
25 increase of experiment time during ten hours (SI Fig. S5), which further confirms that
26 most of CTAB in HMSM can be closely attached on the inner surface of
27 silica-nanochannels and the HMSM-CTAB-supported W/DCH interface can be used
28 repeatedly within a period of time. However, the leakage of aqueous solution from
29 glass tube will happen if the experiment time is much too long. This problem can be
30 solved by the fabrication of HMSM-CTAB-supported organogel-electrode after the
31 gelation of organic phase in the glass tube.
32
33
34
35
36
37
38
39
40
41
42
43
44
45
46
47
48
49
50
51
52
53
54
55
56
57
58
59
60

The insets of Fig. S4A and Fig. S4B further demonstrate that the peak currents (I_p) of CV curves for the IT of FA^- from W to DCH increase with the scan rate (ν) and display a linear dependence on $\nu^{1/2}$. According to the Randles-Sevcik equation,^{18,46} the diffusion coefficient of FA^- in aqueous phase was calculated as about $2.06 \pm 0.1 \times 10^{-5} \text{ cm}^2 \text{ s}^{-1}$ by using HMSM-CTAB. This value is smaller than that obtained by using HMSM ($4.1 \pm 0.1 \times 10^{-5} \text{ cm}^2 \text{ s}^{-1}$), which could be ascribed to the hindrance effect of CTAB in HMSM on the transport of molecules or ions inside the silica-CTAB nanochannels as reported previously.^{56,57} However, it is noteworthy that the I_p corresponding to the IT of FA^- at the HMSM-CTAB-supported W/DCH interface are $\sim 80.6\%$ greater than that obtained by using HMSM. In addition, the peak potentials of CVs corresponding to ITs of FA^- from W to DCH shift positively $\sim 80 \text{ mV}$ for the W/DCH interface supported by HMSM-CTAB instead of HMSM. According to all above IT behaviors of reference ion TMA^+ and FA^- and the previous reports on the measured values transposed to the Galvani potential scale on the basis of the following equations:⁴⁰

$$E_p(FA^-) - \Delta_{DCH}^W \phi^o(FA^-) = E_p(R) - \Delta_{DCH}^W \phi^o(R) \quad (1)$$

$$\Delta G_{tr}^{o,W \rightarrow DCH}(FA^-) = -nF\Delta_{DCH}^W \phi^o(FA^-) \quad (2)$$

where R is the reference ion, TMA^+ , and F is the Faraday constant. As the reference ion used in this work, a value of $\Delta_{DCH}^W \phi^o(TMA^+) = 0.173 \text{ V}$ was used.⁶⁰ The Galvani transfer potential and the Gibbs transfer energy for the direct transfer of FA^- from water to DCH at the HMSM-supported W/DCH interface were respectively calculated as -0.115 V and 11.10 kJ/mol , which are different from the values of -0.015 V and 1.45 kJ/mol obtained at the HMSM-CTAB-supported W/DCH interface, indicating that the CTAB in HMSM can affect the IT reactions occurring at the such meso-W/DCH interface arrays. Yamaguchi et al. reported that HMSM containing CTAB could act as a solid-extraction membrane to efficiently extract anions from aqueous solution into silica-CTAB nanochannels based on an anion-exchange process between anions and the bromide of CTAB involving with the dehydration of anions.⁶¹ Thus, it is possible that

1
2
3
4
5
6
7
8
9
10
11
12
13
14
15
16
17
18
19
20
21
22
23
24
25
26
27
28
29
30
31
32
33
34
35
36
37
38
39
40
41
42
43
44
45
46
47
48
49
50
51
52
53
54
55
56
57
58
59
60

FA⁻ could be extracted into the silica-CTAB nanochannels before IT process, which leads to the preconcentration of FA⁻ in HMSM-CTAB and the corresponding current-enhancement phenomenon. Therefore, as illustrated as Scheme 3A, it is reasonable for FA⁻ to be pre-concentrated and partially dehydrated inside the silica-CTAB nanochannels of HMSM-CTAB before IT process, which results in the corresponding phenomena of current-enhancement and positive potential-shift. Indeed, our recent work has demonstrated that the IT behaviors of some anions occurring at the L/L interface modified by an anion-exchange membrane containing narrow pores are also related to the dehydration processes of anions prior to IT.⁶²

Electrochemical Determinations of FA⁻ at the Meso-W/DCH Interface Arrays by CV and DPV. Since the current response corresponding to the IT of FA⁻ can be enhanced by CTAB, it is necessary to confirm whether such a current-enhancement phenomenon is beneficial to improve the performance of electrochemical detection of FA⁻. Fig. 4A and B show the CVs obtained under the different concentrations of FA⁻ in the aqueous phase at the different W/DCH interfaces supported by HMSM or HMSM-CTAB, respectively. In addition to the different shapes of CVs as discussed above, it can be found from all those CVs that the relationship between the peak currents (I_p^{W-DCH}) corresponding to the IT of FA⁻ from W to DCH and the concentration of FA⁻ (C_{FA}) in aqueous phase exhibit more sensitivity at the HMSM-CTAB-supported W/DCH interface than that at the HMSM-supported W/DCH interface. According to the calibration curves (the insets of Fig. 4A and Fig. 4B) and the Analytical Methods Committee recommendations,⁶³ the values of S and LOD obtained at both of W/DCH interfaces supported by HMSM and HMSM-CTAB are indeed different. As listed in Table 1, the values of S and LOD for the detection of FA⁻ at the HMSM-CTAB-supported W/DCH interface are, respectively, 0.47 $\mu\text{A mM}^{-1}$ and 100 μM , both of which are better than that evaluated at HMSM-supported W/DCH interface (0.37 $\mu\text{A mM}^{-1}$ and 180 μM , respectively), indicating that the current-enhancement phenomenon induced by CTAB was helpful to improve the electrochemical detection of FA⁻ at such meso-W/DCH interface arrays.

1
2
3
4
5
6
7
8
9
10
11
12
13
14
15
16
17
18
19
20
21
22
23
24
25
26
27
28
29
30
31
32
33
34
35
36
37
38
39
40
41
42
43
44
45
46
47
48
49
50
51
52
53
54
55
56
57
58
59
60

Fig. 5A and Fig. 5B show the DPV curves and the corresponding calibration curves obtained under different concentrations of FA⁻ in the aqueous phase at the W/DCH interfaces supported by HMSM or HMSM-CTAB, respectively. Further, it was found that the values of S and LOD for the detection of FA⁻ are also closely related to the surfactants CTAB in HMSM. As list in Table 1, the values of S and LOD for the detection of FA⁻ can be improved from 0.07 $\mu\text{A mM}^{-1}$ and 80 μM (HMSM-supported W/DCH interface) to 0.11 $\mu\text{A mM}^{-1}$ and 40 μM (HMSM-CTAB-supported W/DCH interface). This result further confirms that CTAB significantly influenced the electrochemical detection of FA⁻ at meso-W/DCH interface arrays. Although the values of LOD of FA⁻ obtained at the meso-W/DCH interface arrays by DPV could reach μM -level, but they were still worse than the LOD (nM-level) obtained by non-electrochemical methods⁵ or by the adsorptive stripping voltammetry at the solid electrode.³ Therefore, a key problem was inevitable that LODs of FA⁻ at the meso-W/DCH interface arrays by CV and DPV were still significantly high. The above mentioned problem could be overcome by employing another voltammetric technique with higher sensitivity, DPSV, which has been recently used in the high-sensitive electroanalyses of ions at the water/organogel interface.^{41,42}

Ion-Transfer Behaviors and Electrochemical Detection of FA⁻ at the Meso-Water/Organogel Interface Arrays. In view of the positive role of CTAB for the electrochemical detection of FA as discussed above, the following CV and DPSV experiments mainly focused on the HMSM-CTAB-supported meso-water/organogel interface arrays. As shown as Fig. S6, the IT of FA⁻ across the HMSM-CTAB-supported meso-water/organogel interface arrays under different scan rates produced asymmetric CV curves, namely the peak-shaped waves on forward scan and the steady-state waves on the backward scan, which is inverse to the asymmetric CV curves obtained at the HMSM-supported meso-W/DCH interface arrays. Those inversed asymmetric CVs indicate that the meso-water/organogel interface arrays should form at the membrane surface of HMSM-CTAB due to the complete filling of organogel inside the silica-CTAB nanochannels with the relatively hydrophobic inner

1
2
3 environment,⁵⁶ as shown in Scheme 3B. As a result, on the forward sweep, the egress
4 transfer of FA⁻ from the organogel inside HMSM to the outer aqueous phase is
5 dominated by linear diffusion, which produces a peak-shaped CV response due to the
6 confinement of silica-CTAB nanochannels in HMSM, while the ingress transfer of FA⁻
7 into the organogel phase on the reverse sweep is controlled by radial diffusion, which
8 produces a steady wave. The inset of Fig. S6 shows that the peak currents (I_p) of CV
9 curves for the IT of FA⁻ from organogel to water increase with the scan rate (ν) and
10 display a linear dependence on $\nu^{1/2}$. According to the Randles-Sevcik equation,^{18,46} the
11 diffusion coefficient of FA⁻ in organogel is calculated as about $1.1 \pm 0.1 \times 10^{-5} \text{ cm}^2 \text{ s}^{-1}$,
12 which is smaller than that of FA⁻ in aqueous phase as obtained above owing to the high
13 viscosity of organogel.⁴² Additionally, the transfer potentials of FA⁻ at the
14 HMSM-CTAB-supported meso-water/organogel interface arrays can be evaluated as
15 0.55 V (from the organogel to the aqueous phase) and 0.5 V (from the aqueous phase to
16 the organogel) according to those CV curves, which are the important parameters to
17 fulfill the followed DPSV experiments.

18
19
20
21
22
23
24
25
26
27
28
29
30
31
32 According to the literature,^{41,42} the entire procedure for the electrochemical
33 detection of ions using DPSV technique consisted of three steps, namely
34 preconditioning, preconcentration, and voltammetric analysis. Herein, the
35 preconditioning step was employed for 90 s at the potential of 0.8 V. After that, the
36 accumulation of FA⁻ occurred in the organogel via its transfer across the
37 meso-water/organogel interface arrays at the potential of 0.25 V (the preconcentration
38 step). Finally, the preconcentrated FA⁻ was stripped out of the organic phase using
39 DPSV (the voltammetric analysis step). As far as the preconcentration time, an
40 important factor of DPSV technique, is concerned, Fig. S7 shows that the stripping peak
41 current rapidly increases with the increase in preconcentration time and reaches a
42 plateau after 60 s. Therefore, a preconcentration time of 60 s was selected as an
43 optimum value and employed in all subsequent experiments with an interval of 150 s
44 between each run. In the voltammetric analysis step, as illustrated in Fig. 6, the
45 stripping peak current of DPSV curve increases with the increase in concentration of
46
47
48
49
50
51
52
53
54
55
56
57
58
59
60

1
2
3
4
5
6
7
8
9
10
11
12
13
14
15
16
17
18
19
20
21
22
23
24
25
26
27
28
29
30
31
32
33
34
35
36
37
38
39
40
41
42
43
44
45
46
47
48
49
50
51
52
53
54
55
56
57
58
59
60

FA⁻ in the aqueous phase. Moreover, the calibration curve (the inset of Fig. 6) exhibits a linear increase in current in the concentration range of FA⁻ between 1 and 18 μM, with a high correlation coefficient (0.996) and a saturation effect occurring at higher concentrations. The corresponding values of S and LOD were estimated about 20 μA mM⁻¹ and 0.08 μM at the HMSM-CTAB-supported water/organogel interface, which were obviously better than those values (2 μA mM⁻¹ and 0.2 μM) obtained at HMSM-supported water/organogel interface under the same experimental condition (SI Fig. S8), further illuminating the positive effect of CTAB on the electrochemical detection of FA⁻ at such meso-W/DCH interface arrays as mentioned above. According to all the aforementioned voltammetric results and the data listed in Table 1, it could be inferred that the main electroanalytical performance (S and LOD) based on the IT of FA⁻ at such meso-L/L interface arrays should be closely related with two factors, namely the CTAB self-assembled within the silica nanochannels of HMSM and the different sensitivity of employed voltammetric methods. Undoubtedly, the combination of DPSV technique and additional preconcentration of FA⁻ in the silica-CTAB nanochannels through an anion-exchange process between FA⁻ and the bromide of CTAB in HMSM was expected to provide a competitive method for the detection of FA under physiological conditions.

As a potentially amperometric sensor of FA, the reproducibility and the selectivity of such HMSM-CTAB-supported organogel electrodes were preliminarily investigated. When four HMSM-CTAB-supported organogel electrodes were prepared by using different HMSM-CTAB membranes to examine the same sample, it is found that the peak currents corresponding to the IT of FA⁻ from aqueous phase to organogel are close according to those CVs obtained by using different HMSM-CTAB-supported organogel electrodes (SI Fig. S9) and the relative standard deviation of peak currents is about 1.76%. As a result, such HMSM-CTAB-supported organogel electrodes present the acceptable reproducibility for the determination of FA in view of the relatively low porosity of commercial PET membranes and the complicated structure of pores-in-pores of such HMSMs employed in this work although the pore structure of

PET membrane is random. The selectivity of the amperometric determination of FA was evaluated by the determination of the selectivity coefficients according to the method proposed by Wang⁶⁴ in the presence of some anionic interfering agents, including ClO_4^- , SCN^- , ascorbic acid, AC^- and SO_4^{2-} . As for ascorbic acid, the transfer of ascorbate was not observed at the HMSM-CTAB-supported water/organogel interface, which is similar to the result reported previously.⁴⁰ Also, no transfers of hydrophilic anions, such as AC^- and SO_4^{2-} , could be observed at the same interface. The possible reason should be due to the limitation of electrochemical window and their too high Gibbs transfer energies. The variations induced by the hydrophilic anions on the FA peak currents were less than 4%, which indicates that those hydrophilic anions does not interfere significantly in the determination of FA. As for the relatively hydrophobic interfering anions, ClO_4^- and SCN^- , the parameters evaluated from the linear fitting of I_t as a function of FA^- concentration and the corresponding amperometric selectivity coefficients ($k_{ij}^{\text{amp}} = \frac{\text{Intercept}}{\text{Slope} \cdot C_j}$) defined by Wang⁶⁴ were calculated and list in the Table. 2 according to the plot of I_t as a function of C_{FA} in the presence of interfering anions (SI Fig. S10) and the method as reported previously on the selectivity of amperometric sensors⁶⁴⁻⁶⁶. It is found that the values of the selectivity coefficients are relatively low, which demonstrates such a HMSM-CTAB-supported organogel electrode can be potentially applied as an amperometric sensor for the detection of anionic FA although it is possible for some hydrophilic anions with much high concentration existed in the practical samples to interfere the direct determination of FA in aqueous solution under the physiological conditions.

In order to further examine the practical application of the detection method for FA as-proposed in this study, a kind of commercial FA tablet was analyzed by DPSV technique and HMSM-CTAB-supported organogel electrode. According to the DPSV curve corresponding to the prepared sample solution of FA (SI Fig. S11) and the calibration curve (the inset of Fig. 6), the content of folic acid in the tablet sample is

1
2
3
4
5
6
7
8
9
10
11
12
13
14
15
16
17
18
19
20
21
22
23
24
25
26
27
28
29
30
31
32
33
34
35
36
37
38
39
40
41
42
43
44
45
46
47
48
49
50
51
52
53
54
55
56
57
58
59
60

calculated as 0.393 mg, which was almost in close agreement with the standard value (0.4 mg) of this commercial tablet and that obtained by using lead film electrode.³ Moreover, the recovery ratio and the relative standard deviation were, respectively, evaluated as 92.4 ± 1.40 and 1.52 % (SI Table S1), which demonstrated that such a novel detection method exhibited reliable accuracy and precision for the practical pharmaceutical analysis of FA. Compared with other types of micro-L/L interface arrays supported by the porous membranes of PAA³¹ and PET^{32,40} or silicon chip,³⁴⁻³⁶ the meso-L/L interface arrays supported by such hybrid mesoporous silica membranes can provide not only the meso-sized selectivity for the ion transfer or extraction,⁴⁶ but also a unique strategy to improve the detection sensitivity of anions based on the additional preconcentration of anion in the silica-CTAB nanochannels through an anion-exchange process. Additionally, in view of the well-known silane chemistry,⁶⁷ versatile chemical selectivity of such meso-L/L interface arrays should be more easily fulfilled with comparison to other types of micro-L/L interface arrays after the functionalization of silica rods formed in those HMSMs, which should be significant for the further development of membrane-supported micro-L/L interface arrays as the amperometric ion-sensors with high selectivity. Moreover, those porous membranes with ordered pore structure, such as PAA,^{56,61} can also be applied as the hard templates for the preparation of such HMSMs, which will be helpful for the fabrication of HMSMs-based ion-sensors with more uniform structure and better properties in the future.

Conclusions

In this study, the IT voltammetry of FA at the polarized L/L interface was first investigated and then applied as a novel detection method for FA under physiological conditions. Two types of meso-L/L interface arrays, namely meso-water/1,6-dichlorohexane (W/DCH) and meso-water/organogel interface arrays are supported by using a hybrid mesoporous silica membrane (HMSM) with unique structure of pores-in-pores and employed as the new platforms for the IT voltammetric study. It was found that all the voltammetric responses of CV, DPV, and

1
2
3 DPSV and the corresponding detection limit of FA at such meso-L/L interface arrays
4 are closely related to the CTAB in HMSM, which could be attributed to the
5 preconcentration of FA⁻ in the silica-CTAB nanochannels of HMSM through an
6 anion-exchange process induced by CTAB. Significantly, the limit of detection (LOD)
7 for FA can be improved to nM-level at the HMSM-CTAB supported water/organogel
8 interface by coupling DPSV technique with the additional preconcentration of FA in the
9 silica-CTAB nanochannels. Based on this study, it was expected that the meso-L/L
10 interface arrays supported by HMSM containing ionic surfactant CTAB could provide a
11 unique platform for the IT voltammetric study and the highly-sensitive detection of
12 some biological anions relying on their IT reactions at the L/L interface. In the future,
13 those functionalized HMSMs with uniform micro-structure should be further developed
14 for the fabrication of ion sensors with better properties.
15
16
17
18
19
20
21
22
23
24
25
26
27

28 Acknowledgments

29
30 Financial support from the National Science Foundation of China (21005049) and
31 the Natural Science Foundation of Shanghai, China (No.14ZR1440900) is gratefully
32 acknowledged.
33
34
35
36

37 Notes and References

38
39
40 Electronic Supplementary Information (ESI) available: The scheme of the homemade
41 four-electrode electrochemical cell; DPV curves corresponding to the IT of FA at the
42 HMSM-supported W/DCH interface under different pH values; SEM images of the
43 surface of HMSM after the experiment conducted under the condition of pH~11.0;
44 Continuous CVs corresponding to the IT of FA⁻ at the HMSM-CTAB-supported
45 W/DCH interface; CVs of the IT of FA⁻ across the W/DCH interface supported by
46 HMSM or HMSM-CTAB, as well as the HMSM-CTAB-supported water/organogel
47 interface at different scan rates; Influence of the preconcentration time on the DPSV
48 of FA⁻ at the HMSM-CTAB-supported water/organogel interface; DPSV curves of FA
49
50
51
52
53
54
55
56
57
58
59
60

1
2
3
4 at the HMSM-supported water/organogel interface; CVs corresponding to the IT of FA⁻
5 obtained by using four different HMSM-CTAB-supported organogel electrodes;
6
7 Calibration curve for FA⁻ transfer at the HMSM-CTAB-supported water/organogel
8 interface in the presence of SCN⁻ and ClO₄⁻; DPSV curve of the prepared sample
9 solution of FA; Table of the recovery ratio and the relative standard deviation for the
10 determination of FA in a kind of commercial FA tablet using DPSV technique. See
11 DOI: 10.1039/b000000x/
12
13
14
15
16
17

- 18
19 1 F. H. Nazki, A. S. Sameer and B. A. Ganaie, *Gene*, 2014, 533, 11-20.
20
21 2 A. de Bree, M. van Dusseldorp, I. A. Brouwer, K. H. van het Hof and R. P. M.
22 Steegers-Theunissen, *Eur. J. Clin. Nutr.*, 1997, 51, 643-660.
23
24 3 M. Korolczuk and K. Tyszczyk, *Electroanalysis*, 2007, 19, 1959-1962.
25
26 4 D. Hoegger, P. Morier, C. Vollet, D. Heini, F. Reymond and J. S. Rossier, *Anal.*
27 *Bioanal. Chem.*, 2007, 387, 267-275.
28
29 5 J. E. Young, M. T. Matyska and J. J. Pesek, *J. Chromatogr. A*, 2011, 1218, 2121-2126.
30
31 6 S. D. Garbis, A. Melse-Boonstra, C. E. West and R. B. van Breemen, *Anal. Chem.*,
32 2001, 73, 5358-5364.
33
34 7 S. L. Zhao, H. Y. Yuan, C. Xie and D. J. Xiao, *J. Chromatogr. A*, 2006, 1107, 290-293.
35
36 8 P. Nagaraja, H. Krishna, A. Shivakumar, R. A. Vasantha and D. Rangappa, *Anal.*
37 *Biochem.*, 2002, 307, 316-321.
38
39 9 P. Kalimuthu and S. A. John, *Biosens. Bioelectron.*, 2009, 24, 3575-3580.
40
41 10 K. Zhao, L. Zhao, Y. He, Y. Cai, D. M. Tian, S. L. Zang and Y. Y. Zhang, *J.*
42 *Electroanal. Chem.*, 2012, 667, 105-112.
43
44 11 A. -C. Le Gall and C. M. G. van den Berg, *Anal. Chim. Acta.*, 1993, 282, 459-470.
45
46 12 P. A. M. Farias, M. D. C. Rezende and J. C. Moreira, *IOSR J. Pharm.*, 2012, 2,
47 302-311.
48
49 13 S. Kwee, *Bioelectrochem. Bioenerg.*, 1983, 11, 467-475.
50
51 14 Z. H. Wang, Q. H. Han, J. F. Xia, L. Xia, S. Bi, G. Y. Shi, F. F. Zhang, Y. Z. Xia, Y. H.
52 Li and L. H. Xia, *J. Electroanal. Chem.*, 2014, 726, 107-111.
53
54
55
56
57
58
59
60

- 1
2
3 15 H. H. Girault, *In Electroanalytical Chemistry, A Series of Advances*, A. J. Bard, C. G.
4 Zoski, eds., CRC Press: Boca Raton, 2010; pp 1-104.
5
6
7 16 D. W. M. Arrigan, G. Herzog, M. D. Scanlon, J. Strutwolf, *In Electroanalytical*
8 *Chemistry, A Series of Advances*, Bard, A. J., Zoski, C. G., eds., CRC Press, Boca Raton,
9 2013, pp 105-178.
10
11
12 17 S. Amemiya, Y. Wang, M. V. Mirkin, *In Electrochemistry*, J. D. Wadhawan, R. G.
13 Compton, eds., The Royal Society of Chemistry: Cambridge, 2014, pp 1-43.
14
15
16 18 S. J. Liu, Q. Li and Y. H. Shao, *Chem. Soc. Rev.*, 2011, 40, 2236-2253.
17
18
19 19 G. Taylor and H. H. Girault, *J. Electroanal. Chem.*, 1986, 208, 179-183.
20
21 20 D. Zhan, S. Mao, Q. Zhao, Z. Chen, H. Hu, P. Jing, M. Q. Zhang and Y. H. Shao,
22 *Anal. Chem.*, 2004, 76, 4128-4136.
23
24 21 Y. H. Shao, B. Liu and M. V. Mirkin, *J. Am. Chem. Soc.*, 1998, 120, 12700-12701.
25
26 22 Y. Chen, Z. Gao, F. Li, L. Ge, M. Zhang, D. Zhan and Y. H. Shao, *Anal. Chem.*, 2003,
27 75, 6593-6601.
28
29 23 H. J. Lee, P. D. Beattie, B. J. Seddon, M. D. Osborne and H. H. Girault, *J.*
30 *Electroanal. Chem.*, 1997, 440, 73-82.
31
32 24 M. D. Osborne and H. H. Girault, *Electroanalysis*, 1995, 7, 714-721.
33
34 25 U. Nestor, H. Wen, G. Girma, Z. Mei, W. Fei, Y. Yang, C. Zhang and D. Zhan, *Chem.*
35 *Commun.*, 2014, 50, 1015-1017.
36
37 26 Q. S. Qian, G. S. Wilson, K. Bowman-James and H. H. Girault, *Anal. Chem.*, 2001,
38 73, 497-503.
39
40 27 Q. S. Qian, G. S. Wilson and K. Bowman-James, *Electroanalysis*, 2004, 16,
41 1343-1350.
42
43 28 G. C. Lillie, R. A. W. Dryfe and S. M. Holmes, *Analyst*, 2001, 126, 1857-1860.
44
45 29 S. Senthilkumar, R. A. W. Dryfe and R. Saraswathi, *Langmuir*, 2007, 23, 3455-3461.
46
47 30 M. Platt, R. A. W. Dryfe and E. P. L. Roberts, *Langmuir*, 2003, 19, 8019-8025.
48
49 31 X. Lu, T. Wang, X. Zhou, Y. Li, B. Wu and X. Liu, *J. Phys. Chem C*, 2011, 115,
50 4800-4805.
51
52 32 H. J. Lee and H. H. Girault, *Anal. Chem.*, 1998, 70, 4280-4285.
53
54
55
56
57
58
59
60

- 1
2
3 33 M. M. Hossain, S. H. Lee, H. H. Girault, V. Devaud and H. Lee, *J. Electrochim. Acta*,
4 2012, 82, 12-18.
5
6
7 34 E. Alvarez de Eulate and D. W. M. Arrigan, *Anal. Chem.* 2012, 84, 2505-2511.
8
9 35 S. O' Sullivan and D. W. M. Arrigan, *Anal. Chem.*, 2013, 85, 1389-1394.
10
11 36 J. Strutwolf, M. D. Scanlon and D. W. M. Arrigan, *Analyst*, 2009, 134, 148-158.
12
13 37 M. D. Scanlon, J. Strutwolf and D. W. M. Arrigan, *Phys. Chem. Chem. Phys.*, 2010,
14 12, 10040-10047.
15
16 38 A. Berduque, R. Zazpe and D. W. M. Arrigan, *Anal. Chim. Acta*, 2008, 611, 156-162.
17
18 39 J. Ribeiro, A. I. M. Miranda, F. Silva and C. M. Pereira, *Phys. Chem. Chem. Phys.*,
19 2010, 12, 15190-15194.
20
21 40 J. Ribeiro, F. Silva and C. M. Pereira, *Anal. Chem.*, 2013, 85, 1582-1590.
22
23 41 M. D. Scanlon, G. Herzog and D. W. M. Arrigan, *Anal. Chem.*, 2008, 80, 5743-5749.
24
25 42 C. J. Collins and D. W. M. Arrigan, *Anal. Chem.*, 2009, 81, 2344-2349.
26
27 43 E. Alvarez de Eulate, S. O'Sullivan, S. Fletcher, P. Newsholme and D. W. M.
28 Arrigan, *Chem. Asian J.*, 2013, 8, 2096-2101.
29
30 44 S. O' Sullivan, E. Alvarez de Eulate, Y. H. Yuen, E. Helmerhorst and D. W. M.
31 Arrigan, *Analyst*, 2013, 138, 6192-6196.
32
33 45 J. Strutwolf and D. W. M. Arrigan, *Anal. Bioanal. Chem.*, 2010, 398, 1625-1631.
34
35 46 Y. Chen, S. J. Bian, K. Gao, Y. Y. Cao, H. Q. Wu, C. X. Liu, X. H. Jiang and X. L.
36 Sun, *J. Membr. Sci.*, 2014, 457, 9-18.
37
38 47 L. Huang, Y. Chen, S. Bian, Y. Huang, Z. Tian and D. Zhan, *Chem. Eur. J.*, 2014, 20,
39 724-728.
40
41 48 H. Katano, H. Tatsumi and M. Senda, *Talanta*, 2004, 63, 185-193.
42
43 49 M. J. Akhtar, M. A. Khan and I. Ahmad, *J. Pharm. Biomed. Anal.*, 1999, 19,
44 269-275.
45
46 50 A. Tyagi and A. Penzkofer, *Chem. Phys.*, 2010, 367, 83-92.
47
48 51 M. Poe, *J. Biol. Chem.*, 1977, 252, 3724-3728.
49
50 52 Z. Wu, X. X. Li, C. Y. Hou and Y. J. Qian, *Chem. Eng. Data*, 2010, 55, 3958-3961.
51
52 53 M. Fertani-Gmati and M. Jemal, *Thermochim. Acta*, 2011, 513, 43-48.
53
54 54 K. Elisa, L. Clara, A. Isabel and M. Fatima, *Can. J. Physiol. Pharmacol.*, 2006, 84,
55
56
57
58
59
60

1
2
3 247-255.

4
5 55 R. A.W. Dryfe and Brett Kralj, *Electrochem. Commun.*, 1999, 1, 128-130.

6
7 56 A. Yamaguchi, M. M. Mekawy, Y. Chen, S. Suzuki, K. Morita and N. J. Teramae, *J.*
8
9 *Phys. Chem. B*, 2008, 112, 2024-2030.

10
11 57 Y. Chen, H. Wu, S. Gan, Y. Wang and X. Sun, *J. Membr. Sci.*, 2012, 403-404,
12
13 94-100.

14
15 58 T. Kasahara, N. Nishi, M. Yamamoto and T. Kakiuchi, *Langmuir*, 2004, 20,
16
17 875-881.

18
19 59 J. Strutwolf, J. A. Manzanares and D. E. Williams, *Electrochem. Commun.*, 1999, 1,
20
21 139-144.

22
23 60 H. Katano and M. Senda, *Anal. Sci.*, 2001, 17, 1207-1209.

24
25 61 A. Yamaguchi, J. Watanabe, M. M. Mahmoud, R. Fujiwara, K. Morita, T. Yamashita,
26
27 Y. Amino, Y. Chen, L. Radhakrishnan and N. Teramae, *Anal. Chim. Acta*, 2006, 556,
28
29 157-163.

30
31 62 D. P. Hu, H. H. Wang, K. Gao, X. H. Jiang, M. Wang, Y. F. Long and Y. Chen, *RSC*
32
33 *Adv.*, 2014, 4, 57035-57040.

34
35 63 J. Mocak, A. M. Bond, S. Mithell and G. Scollary, *Pure Appl. Chem.*, 1997, 69,
36
37 297-328.

38
39 64 J. Wang, *Talanta*, 1994, 41, 857-863.

40
41 65 J. A. Ribeiro, F. Silva and C. M. Pereira, *Talanta*, 2012, 88, 54-60.

42
43 66 J. A. Ribeiro, F. Silva and C. M. Pereira, *Electroanalysis*, 2013, 25, 2331-2338.

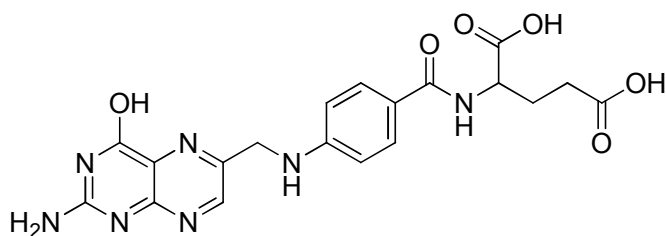
44
45 67 M. Barboiu, A. Cazacu, M. Michau, R. Caraballo, C. A-Herault and A. P-Banu,
46
47 *Chem. Eng. Process.*, 2008, 47, 1044-1052.
48
49
50
51
52
53
54
55
56
57
58
59
60

Table 1 Analytical results for the detection of FA⁻, in the linear range of concentration used, using CV, DPV, and DPSV techniques under physiological conditions (pH~7.2).

Membrane	Detection technique	Linear range/mM (N=5)	Slope/ $\mu\text{A mM}^{-1}$	Intercept/ μA	R	LOD/ μM
HMSM	CV	0.25-1.5	0.37	-0.04	0.990	180
HMSM-CTAB	CV	0.25-1.5	0.47	-0.07	0.992	100
HMSM	DPV	0.25-1.5	0.07	-0.011	0.993	80
HMSM-CTAB	DPV	0.25-1.5	0.11	-0.015	0.992	40
HMSM	DPSV	0.001-0.024	2	0.16	0.996	0.2
HMSM-CTAB	DPSV	0.001-0.018	20	0.19	0.996	0.08

Table 2. The parameters evaluated from the linear fitting of I_t as a function of FA^- concentration and the corresponding amperometric selectivity coefficients

Ion	Slope ($\mu A \mu M^{-1}$)	Intercept (μA)	k_{ij}^{amp}
ClO_4^-	0.0458	0.296	6.46×10^{-4}
SCN^-	0.0473	0.396	8.37×10^{-4}

Scheme 1. Molecular structure of folic acid.**Scheme 2.** Schematic representation of the electrochemical cells used in this study.

Cell 1



Cell 2

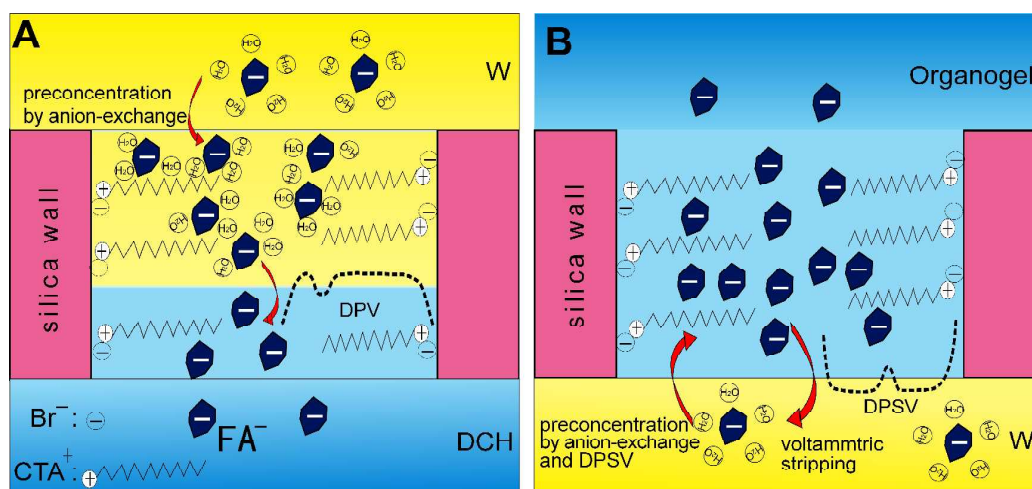
**Scheme 3.** Scheme of the ion-transfer voltammetric determination of FA⁻ at the HMSM-CTAB-supported meso-W/DCH (A) and meso-water/organogel (B) interface by using DPV and DPSV.

Figure captions:

Fig. 1 SEM images of the surface of (A) bare PET membrane and (B) PET-templated HMSM. The insets are the corresponding SEM images of selected region.

Fig. 2 CVs obtained at the W/DCH interface supported by (A) HMSM and (B) HMSM-CTAB in the absence of TMA⁺ (dashed line) and presence of 1 mM TMA⁺ (solid line) at scan rate (ν): 5 mV s⁻¹.

Fig. 3 CVs obtained at the W/DCH interface supported by (A) HMSM and (B) HMSM-CTAB in the absence of FA⁻ (dashed line) and presence of 1 mM FA⁻ (solid line) at scan rate (ν): 5 mV s⁻¹.

Fig. 4 CVs of FA⁻ across the W/DCH interfaces supported by (A) HMSM and (B) HMSM-CTAB at the ν of 5 mV s⁻¹ at increasing concentrations of 0, 0.25, 0.5, 0.75, 1, and 1.5mM (from inner CVs to outer CVs). The insets in (A) and (B) are the corresponding plots of peak current for FA⁻ from W to DCH vs. the concentration of FA (C) in aqueous solution.

Fig. 5 DPVs collected at (A) the HMSM-supported and (B) the HMSM-CTAB-supported W/DCH interface for different concentrations of FA⁻ (0 (blank experiment), 0.25, 0.5, 0.75, 1, and 1.5mM (from top to bottom)) . The insets in (A) and (B) are the corresponding plots of peak current for FA⁻ from W to DCH vs. the concentration of FA (C) in aqueous solution.

Fig. 6 DPSV of FA⁻ at the HMSM-CTAB-supported water/organogel interface: DPSV response of 1, 3, 5, 9, 18, 24, 32, and 42 μ M FA⁻ (from bottom to top). Inset: calibration curve of peak current vs. concentration of FA.

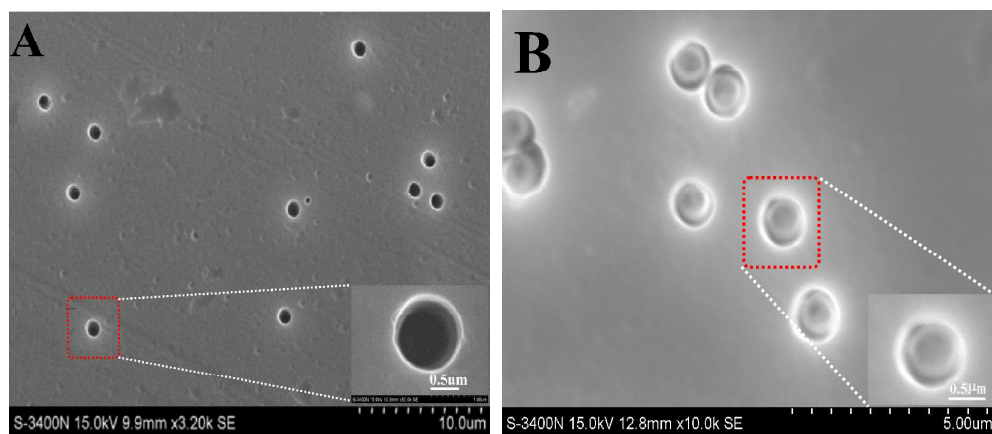


Fig. 1

1
2
3
4
5
6
7
8
9
10
11
12
13
14
15
16
17
18
19
20
21
22
23
24
25
26
27
28
29
30
31
32
33
34
35
36
37
38
39
40
41
42
43
44
45
46
47
48
49
50
51
52
53
54
55
56
57
58
59
60

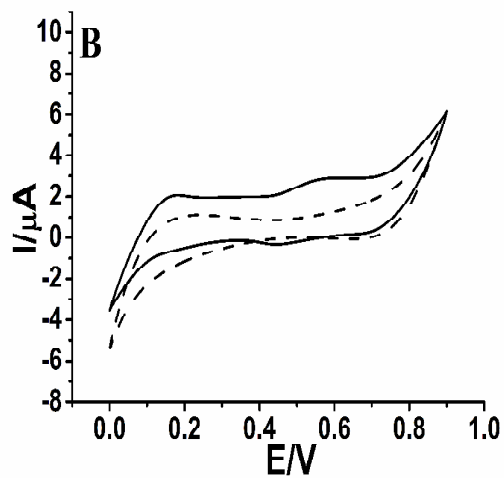
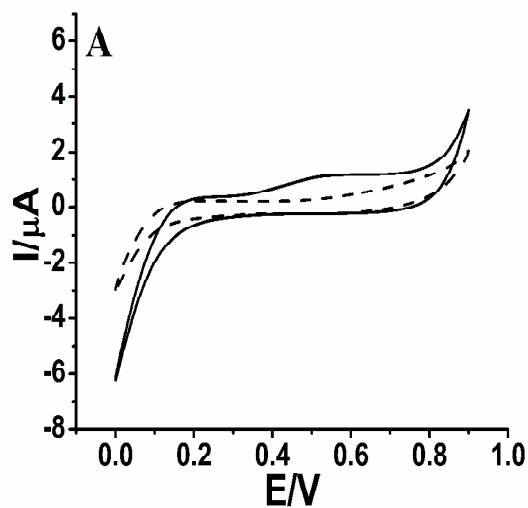


Fig. 2

1
2
3
4
5
6
7
8
9
10
11
12
13
14
15
16
17
18
19
20
21
22
23
24
25
26
27
28
29
30
31
32
33
34
35
36
37
38
39
40
41
42
43
44
45
46
47
48
49
50
51
52
53
54
55
56
57
58
59
60

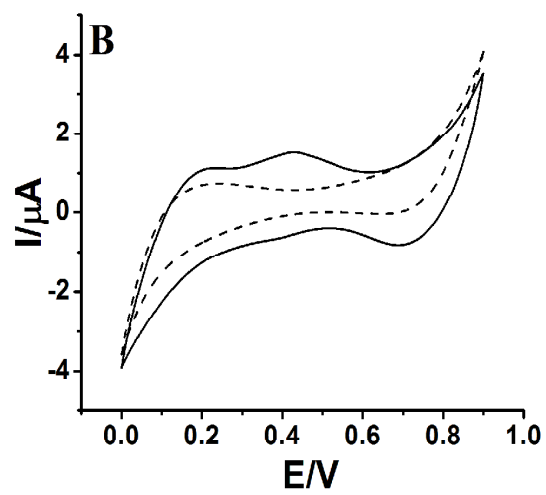
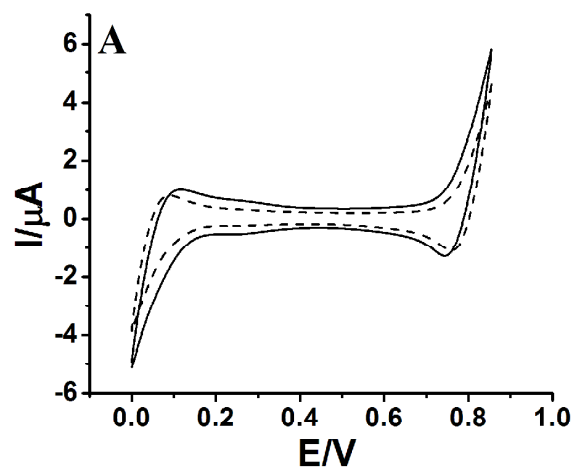
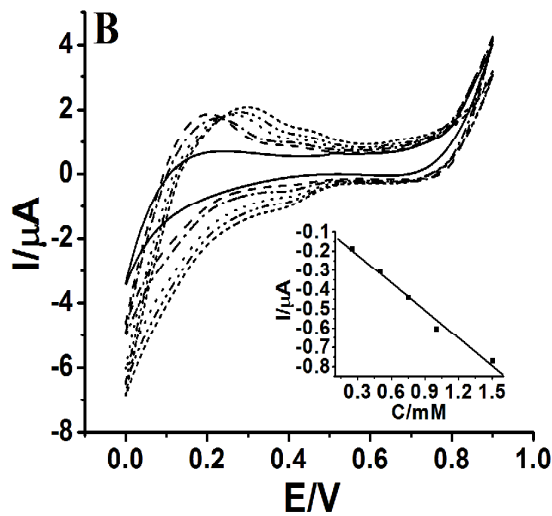
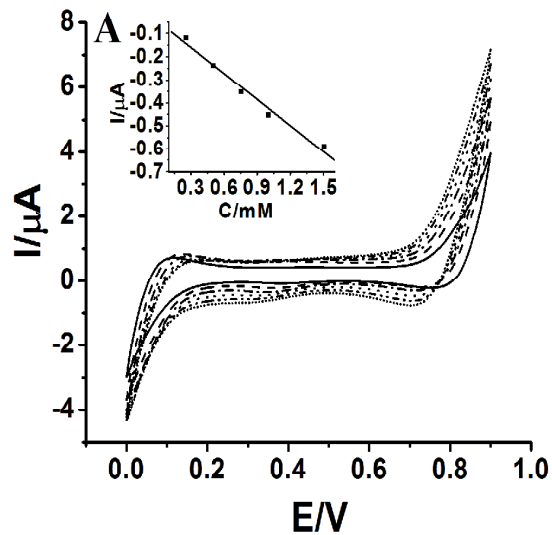


Fig. 3



46
47
48
49
50
51
52
53
54
55
56
57
58
59
60

Fig. 4

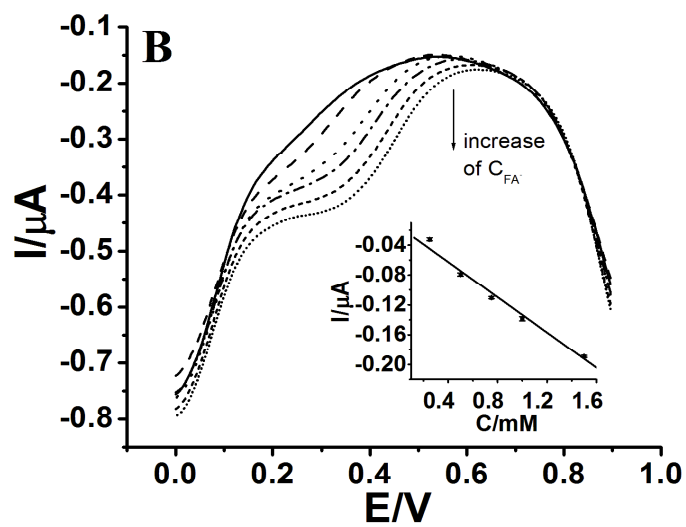
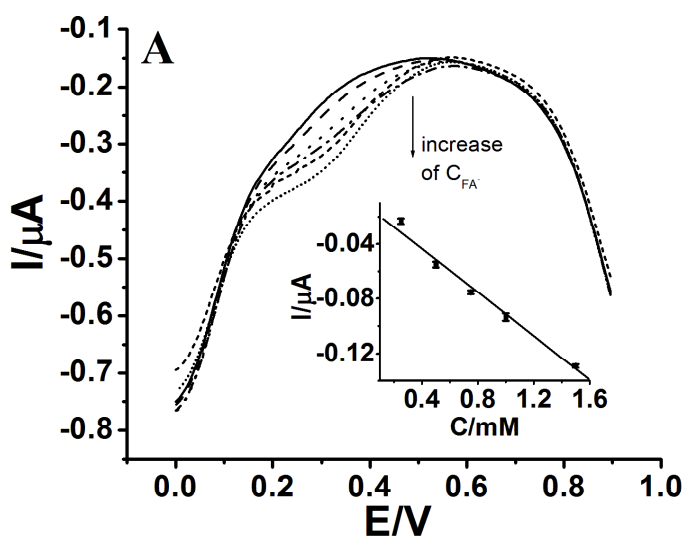


Fig. 5

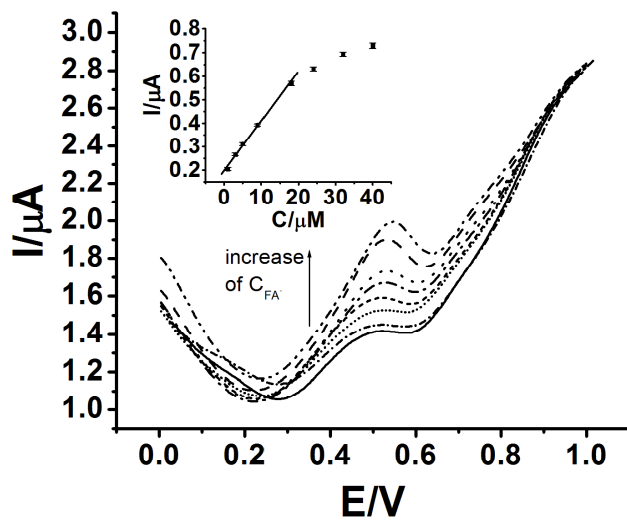


Fig. 6

1
2
3
4
5
6
7
8
9
10
11
12
13
14
15
16
17
18
19
20
21
22
23
24
25
26
27
28
29
30
31
32
33
34
35
36
37
38
39
40
41
42
43
44
45
46
47
48
49
50
51
52
53
54
55
56
57
58
59
60